PROCEEDINGS OF SCIENCE

^{44}Ti and ^{56}Ni in core-collapse supernovae

Georgios Magkotsios*[ab], Francis X. Timmes[abc], Michael Wiescher[b], Christopher L. Fryer[ad], Aimee Hungerford[ad], Patrick Young[ac], Michael E. Bennet[ae], Steven Diehl[adf], Falk Herwig[aeg], Raphael Hirschi[ae], Marco Pignatari[abe] and Gabriel Rockefeller[ad]

[a] *The NuGrid Collaboration*
[b] *Joint Institute for Nuclear Astrophysics, University of Notre Dame, IN, 46556, USA*
[c] *School of Earth and Space Exploration, Arizona State University, Tempe, AZ 85287, USA*
[d] *Computational Methods (CCS-2), Los Alamos National Laboratory, Los Alamos, NM, 87544, USA*
[e] *Astrophysics Group, Keele University, ST5 5BG, UK*
[f] *Theoretical Astrophysics Group (T-6), Los Alamos National Laboratory, Los Alamos, NM, 87544, USA*
[g] *Dept. of Physics & Astronomy, Victoria, BC, V8W 3P6, Canada*
E-mail: gmagkots@nd.edu

We investigate the physical conditions where ^{44}Ti and ^{56}Ni are created in core-collapse supernovae. In this preliminary work we use a series of post-processing network calculations with parameterized expansion profiles that are representative of the wide range of temperatures, densities and electron-to-baryon ratios found in 3D supernova simulations. Critical flows that affect the final yields of ^{44}Ti and ^{56}Ni are assessed.

10th Symposium on Nuclei in the Cosmos
July 27 - August 1 2008
Mackinac Island, Michigan, USA

*Speaker.

PoS(NIC X)112

1. Understanding the mechanisms that produce ^{44}Ti

Cassiopeia A is still the only supernova remnant with an unambiguous detection of ^{44}Ti [5, 6, 10, 9]. Various arguments have been suggested to account for the apparent paucity of such detections. In this work we examine if thermodynamic pathways and nuclear physics responsible for the creation and annihilation of ^{44}Ti can be one of the reasons why there are so few gamma-ray line detections of ^{44}Ti.

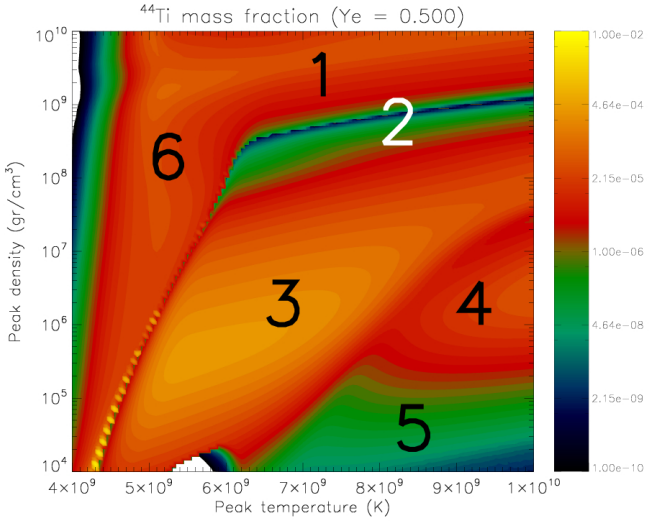

Figure 1: Contour plot of ^{44}Ti final yields as a function of temperature and density for adiabatic expansions. The numbers signify the various regimes for ^{44}Ti nucleosynthesis.

The temperature-density plane of interest for ^{44}Ti is shown in Fig. 1. Each point in the plane represents the initial temperature and density of a material initially composed with an electron fraction of Y_e=0.5. Each point in the plane was then evolved along an adiabatic expansion profile under the assumption of a constant radiation entropy $T^3/\rho \sim$ constant. Colors in the plot correspond to the final ^{44}Ti yields, after adiabatic expansion has cooled the material to the point where nuclear reactions cease. The numbered regions correspond to different evolutionary mechanisms. Of particular interest is the "chasm" of region 2 where very little ^{44}Ti is produced. For each region, only certain reactions affect the yields of ^{44}Ti and ^{56}Ni:

1. Fast freeze-out from NSE. Abundance largely determined from Q-values.
2. Chasm region: Passage from NSE to QSE. Reactions: ^{44}Ti$(\alpha,\mathrm{p})^{47}$V, ^{20}Ne$(\alpha,\mathrm{p})^{23}$Na, ^{21}Na$(\alpha,\mathrm{p})^{24}$Mg, ^{20}Ne$(\mathrm{p},\gamma)^{21}$Na
3. Normal α-rich freeze-out: ^{56}Ni dominates. Reactions: $3\alpha \rightarrow {}^{12}$C, ^{44}Ti$(\alpha,\mathrm{p})^{47}$V, ^{20}Ne$(\alpha,\mathrm{p})^{23}$Na, ^{21}Na$(\alpha,\mathrm{p})^{24}$Mg, ^{45}V$(\mathrm{p},\gamma)^{46}$Cr, ^{57}Ni$(\mathrm{p},\gamma)^{58}$Cu
4. α- and p-rich freeze-out. Reactions: $3\alpha \rightarrow {}^{12}$C, ^{45}V$(\mathrm{p},\gamma)^{46}$Cr, ^{44}Ti$(\mathrm{p},\gamma)^{45}$V, ^{41}Sc$(\mathrm{p},\gamma)^{42}$Ti, ^{43}Sc$(\mathrm{p},\gamma)^{44}$Ti, ^{40}Ca$(\mathrm{p},\gamma)^{41}$Sc, ^{40}Ca$(\alpha,\mathrm{p})^{43}$Sc

5. Photodisintegration regime: n, p and α dominate

6. Incomplete silicon burning: ^{28}Si rich

The importance of these reactions was determined from analysis of the flows in a sensitivity survey.

2. Chasm shift between expansion profiles for symmetric matter

Next we consider the effect of two different parameterizations on how material cools down, the adiabatic expansion pathway described above (left image in Fig. 2) and a power-law profile derived from 3D simulations of the supernova explosion (right image in Fig. 2). In general, for any given Y_e, a power-law expansion profile shifts the ^{44}Ti chasm to lower densities. Points from multi-dimensional supernova simulations are overlayed on these two ^{44}Ti maps, and suggest that core-collapse supernovae may populate the region of parameter space where very little ^{44}Ti is produced.

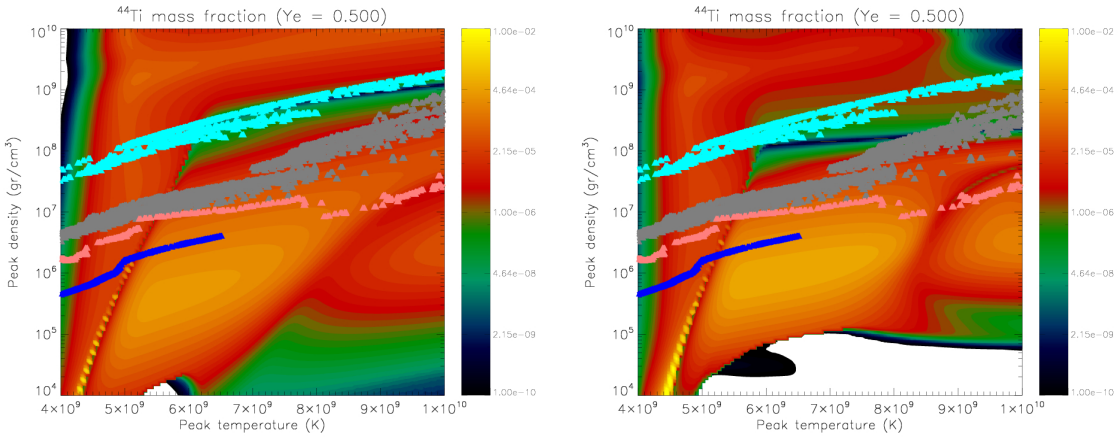

Figure 2: ^{44}Ti contour plots for two expansion profiles. The contour plot to the left is for an adiabatic expansion, while the one to the right is for a power-law expansion. The embedded points correspond to conditions met in supernovae simulations. The cyan ones are based on a rotating MHD star, the grey on a rotating 2D explosion model, the pink are for a gamma-ray burst model and the blue ones on a model specifically for Cassiopeia A.

The reaction that accounts for most of the chasm's location is ^{44}Ti$(\alpha,\mathrm{p})^{47}$V. This reaction controls a small-scale equilibrium cycle which keeps ^{44}Ti in the large-scale silicon group QSE cluster. The reaction's equilibrium persistence decreases the ^{44}Ti mass fraction (Fig. 3). For appropriate initial conditions, the expansion timescale is slow enough that this equilibrium persists until the end of nucleosynthesis. For these conditions, ^{44}Ti will be depleted and a chasm appears.

The ^{44}Ti$(\alpha,\mathrm{p})^{47}$V goes out of its equilibrium cycle at a threshold temperature of $T_9 \sim 3$ GK. Since the timescales for different expansion profiles are different, the density at the point in time when this threshold temperature is reached will differ. Different densities when this threshold temperature is reached imply different initial densities for the same initial temperature. The chasm is thus located at lower initial densities for longer expansion timescales.

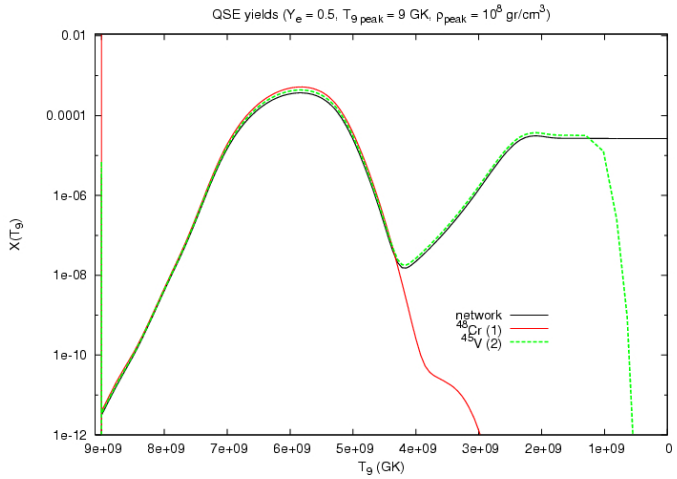

Figure 3: ^{44}Ti mass fraction as a function of temperature. The black curve is the outcome of a network code for a typical α-rich freeze-out. The red curve assumes that ^{44}Ti belongs to the local cluster of the N = 22 and N = 24 isotones, connected by (α, p) reactions. ^{48}Cr is the reference isotope. The green curve assumes that this equilibrium between the isotones has broken, and ^{44}Ti is in equilibrium only with certain isotopes along the N = 22 isotone. ^{45}V is the reference isotope in this case.

3. Calculations for asymmetric matter

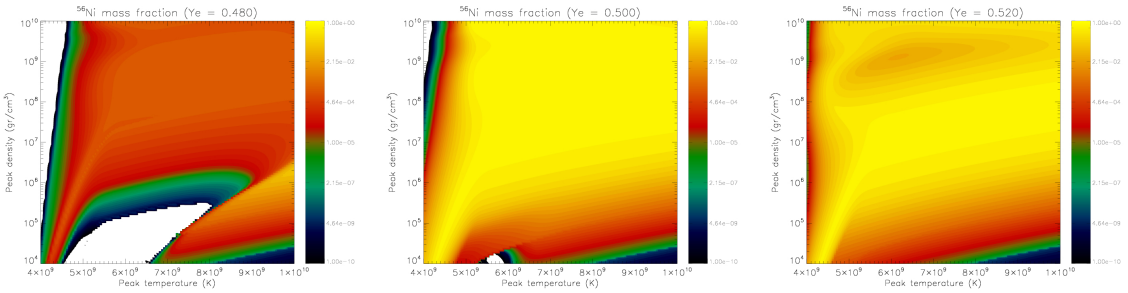

Figure 4: ^{56}Ni contour plots for adiabatic expansions with initial electron fraction $Y_e = 0.48$ (left), $Y_e = 0.50$ (middle) and $Y_e = 0.52$ (right).

The yields for ^{44}Ti and ^{56}Ni are sensitive to the initial value of the electron fraction Y_e, which we study for the the first time. In general, major flows tend to focus along isotopes whose proton to nucleon ratio is equal to the current value of Y_e. Thus, major flows will go through ^{44}Ti and ^{56}Ni for $Y_e = 0.5$, because the number of protons equals the number of neutrons for both isotopes.

As is well known, ^{56}Ni dominates the final compositions when $Y_e = 0.5$ (Fig. 4), because of its relatively high binding energy. For $Y_e < 0.5$ the major flows proceed towards more neutron rich, heavier nuclei and ^{56}Ni does not dominate the final composition. For $Y_e > 0.5$, instead of being dominated by the Fe-peak nuclei with the largest binding energy per nucleon that have a proton to nucleon ratio close to the prescribed electron fraction, proton-rich material minimizes its Helmholtz free energy by being mainly composed of ^{56}Ni and free protons [7].

Fig. 5 shows the ^{44}Ti yields for two different values of Y_e. For $Y_e < 0.5$, it is bypassed by the major flows and hence underproduced. For $Y_e > 0.5$, although it is bypassed again, weak interactions with a halflife shorter to the expansion timescale restore it mass fraction. These reactions include primarily $^{44}V(e^-,\nu_e)^{44}Ti$ and $^{42}Ti(e^-,\nu_e)^{42}Sc$. Additionally, $^{39}Ca(e^-,\nu_e)^{39}K$ and $^{43}Ti(e^-,\nu_e)^{43}Sc$ seem to affect the yield for ^{44}Ti.

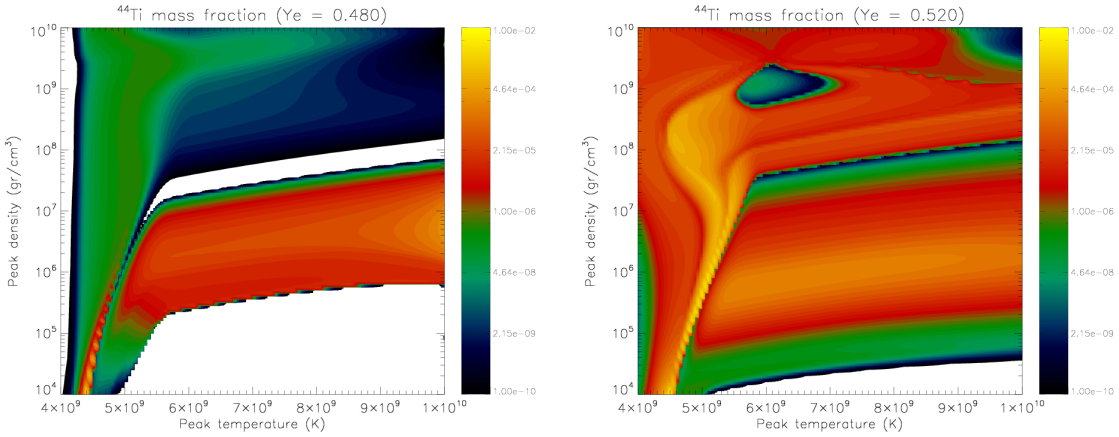

Figure 5: ^{44}Ti contour plots for $Y_e = 0.48$ (left) and $Y_e = 0.52$ (right). Power-law expansions are used for both contours.

References

[1] R. Diehl and F. X. Timmes, *Gamma-Ray Line Emission From Radioactive Isotopes In Stars And Galaxies*, *PASP*, 110, 637 (1998)

[2] W. R. Hix and F.-K. Thielemann, *Silicon Burning. I. Neutronization And The Physics Of Quasi-Equilibrium* ,*ApJ*, 460, 869 (1996)

[3] W. R. Hix and F.-K. Thielemann, *Silicon Burning. II. Quasi-Equilibrium And Explosive Burning*, *ApJ*, 511, 862 (1999)

[4] A.L. Hungerford, C.L. Fryer, G. Magkotsios F.X. Timmes, P.A. Young, *Explosive Nucleosynthesis Trends in Core-Collapse Supernovae*, in preparation (2009)

[5] A. Iyudin, et al., *COMPTEL Observations Of ^{44}Ti Gamma-Ray Line Emission From CAS A*, *A&A*, 284, L1 (1994)

[6] A. Iyudin, *^{44}Ti Decay Gamma-Ray Emission From Young Galactic Supernova Remnants*, *Nuc. Phys. A*, 654, 900c (1997)

[7] I. R. Seitenzahl, F. X. Timmes, A. Marin-Laflèche, E. Brown, G. Magkotsios, J. Truran, *Proton-Rich Nuclear Statistical Equilibrium*, *ApJL*, in press [astro-ph - arXiv:0808.2033] (2008)

[8] L.-S. The, D.D. Clayton, L. Jin, B.S. Meyer, *Nuclear Reactions Governing the Nucleosynthesis of ^{44}Ti*, *ApJ*, 504, 500 (1998)

[9] L. S. The, et al., *Are ^{44}Ti-Producing Supernovae Exceptional?*, *A&A*, 450, 1037 (2006)

[10] Vink, J., et al., *Detection Of The 67.9 And 78.4 keV Lines Associated With The Radioactive Decay Of ^{44}Ti In Cassiopeia A*, *ApJL*, 560, L79 (2001)